Available online at www.sciencedirect.com

ScienceDirect

Energy Procedia 94 (2016) 523 – 530

Energy Procedia

13th Deep Sea Offshore Wind R&D Conference, EERA DeepWind'2016, 20-22 January 2016, Trondheim, Norway

A coupled floating offshore wind turbine analysis with high-fidelity methods

V. Leble, G.N. Barakos*

School of Engineering, James Watt South Building, University of Glasgow, Glasgow G12 8QQ, Scotland, UK

Abstract

This paper presents results of numerical computations for floating off-shore wind turbines using, as an example, a machine of 10-MW rated power. The hydrodynamic loads on the support platform are computed using the Smoothed Particle Hydrodynamics method, which is mesh-free and represents the water and floating structures as a set of particles. The aerodynamic loads on the rotor are computed using the Helicopter Multi-Block flow solver. The method solves the Navier-Stokes equations in integral form using the arbitrary Lagrangian-Eulerian formulation for time-dependent domains with moving boundaries. The motion of the floating offshore wind turbine is computed using a Multi-Body Dynamic Model of rigid bodies and frictionless joints. Mooring cables are modelled as a set of springs and dampers. The loosely coupled algorithm used in this work is described in detail and the obtained results are presented.

Peer-review under responsibility of SINTEF Energi AS

Keywords: Offshore wind turbine; floating; CFD; SPH; multi-body; dynamics; HMB3

1. Introduction

Current trends suggest large development of on-shore wind turbine size and power capacity. Due to the fact that many high potential sites on land are already occupied, and others are hard to utilise owing to *e.g.* difficult access, high altitude *etc.*, a growing trend is to exploit the offshore wind potential and take advantage of the available space and steady winds. In the first six months of 2015 alone, Europe fully grid connected 584 commercial offshore wind turbines with a combined capacity of 2.3GW, and those are bottom-fixed machines. As of today, offshore wind represents 10% of the annual wind energy installations across Europe[1,2]. Estimates for the year 2030 predict up to 11.3% coverage of total European electricity demand by offshore wind[3]. Similar trends are seen in the US, where onshore and offshore wind energy can provide up to 20% of the US electricity by 2030[4].

Over the years offshore wind farms have moved further from the shore and into deeper waters. At the end of 2014, the average water depth of grid connected wind farms was about 23m and the average distance to shore about 33km.

* Corresponding author. Tel.: +44(0)-141-330-4071.
E-mail address: george.barakos@glasgow.ac.uk

Peer-review under responsibility of SINTEF Energi AS
doi:10.1016/j.egypro.2016.09.229

Projects under construction, consented and planned, confirm that average water depths and distances to shore are likely to increase[5]. Shallow water regions suitable for constructing seabed-fixed, offshore wind turbines are limited, and for sea depths exceeding $30 - 60m$, floating structures become more economic. Hence, emphasis is placed on the development of floating offshore wind turbines (FOWTs) with several prototypes already operational across the world[5].

Unlike onshore machines, the FOWT is a highly dynamic system subjected to the wind and wave loads and only constrained by mooring. Further, the rotor frequency is low due to the large size of the blades, and wave frequencies may come close or coincide with the rotational frequency of the rotor. Therefore, it is important to develop a method for the analysis of this air-structure-water system. The purpose of this paper is to present such an algorithm and obtained demonstration results. For this, the Helicopter Multi-Block (HMB3) flow solver[6] is used to solve for the aerodynamic forces acting on the wind turbine (WT) blades. Hydrodynamic forces on the support platform are solved using the Smoothed Particle Hydrodynamics (SPH) method [7,8]. Both solvers are coupled by exchanging information while the FOWT is represented by a lumped mass model.

2. Numerical methods

The HMB3 code is a 3D multi-block structured solver and solves the Navier-Stokes equations in the 3D Cartesian frame of reference. HMB3 solves the Navier-Stokes equations in integral form using the arbitrary Lagrangian-Eulerian formulation for time-dependent domains with moving boundaries [e.g.9–11]. The solver uses a cell-centred finite volume approach combined with an implicit dual-time method[12]. The HMB3 solver has a library of turbulence closures including several one- and two- equation turbulence models, and turbulence simulation is also possible using either the Large-Eddy or the Detached-Eddy simulation approach[13].

The water is modelled with the SPH method[7]. Each SPH particle represents the volume of the fluid and moves according to the Navier-Stokes equations solved in the Lagrangian form. SPH offers a variety of advantages for fluid modelling, particularly those with a free surface and moving bodies. Due to the Lagrangian nature of the SPH method, the free surface requires no special treatment. Further, submerged bodies can be represented with particles. Therefore, it is natural for the method to include floating objects.

The motion of the FOWT components is computed with a multi-body model (MBDM) of rigid bodies and frictionless joints. Mooring cables are modelled as a set of springs and dampers, according to Savenije [14]. The coordinate partitioning method [15,16] is used to solve the resulting system of mixed differential-algebraic equations. The time integration scheme is explicit with various methods up to the Runge-Kutta method of fourth order. The non-linear position equations are solved using a Newton-Raphson method with exact analytical Jacobian.

All solvers were validated separately before coupling. The HMB3 CFD solver has so far been validated for several wind turbine cases, including the NREL Annex XX experiments [17], and the pressure and PIV data of the MEXICO project [18]. The SPH method was validated against the experiments of Greenhow and Lin [19] for the high speed entry of a half-buoyant solid cylinder into calm water. The MBDM was validated using simple mechanical systems of known solutions [16] like 2D and 3D slider-crank mechanisms and gyroscopic wheels [20].

In the present work, the communication between the MBDM, SPH and HMB3 was established through the Message Passing Interface (MPI). Due to the Lagrangian nature of the SPH method, the submerged bodies can be represented with particles and do not require specific coupling. Therefore, by utilising MPI, the MBDM substituted the body motion routines of the SPH solver and reduced the number of coupled codes to two - SPH and HMB3. This implies that MBDM is advancing in time with the same integration scheme as SPH using a symplectic method in this case [21].

2.1. Coupling algorithm and its implementation

Different coupling methods have been extensively studied during the past two decades. The multi-physics problem with adjacent domains can be simulated in a monolithic or in a partitioned way. The former refers to the flow equations and structural equations being solved simultaneously, while the latter means that they are solved separately. Considering that two validated solvers (HMB3 and SPH) are available, the emphasis is placed on partitioned algorithms.

The partitioned coupling can be weak or strong. If the coupling scheme does not involve Jacobians relating the solutions of the two solvers, the scheme is called weak or loose. Explicit coupling schemes, as the one used in this work, are weak. On the other hand, if a Jacobian is employed, the scheme is called strong or tight, as the solution is equivalent to what would be achieved by a monolithical formulation [22].

In the present paper, a weakly coupled approach is employed, namely the parallel conventional staggered method shown in Figure 1(a). SPH employs time step of $\Delta t_{SPH} = 2 \cdot 10^{-4} s$, whereas HMB3 employs time step of $\Delta t_{HMB3} = 2 \cdot 10^{-2} s = 100 \Delta t_{SPH}$. The small time step for the SPH method is required by the explicit integration scheme. The HMB3 solver employs an implicit dual-time method [12] that is superior for larger time steps. Synchronisation of the solvers is performed at the end of each CFD step.

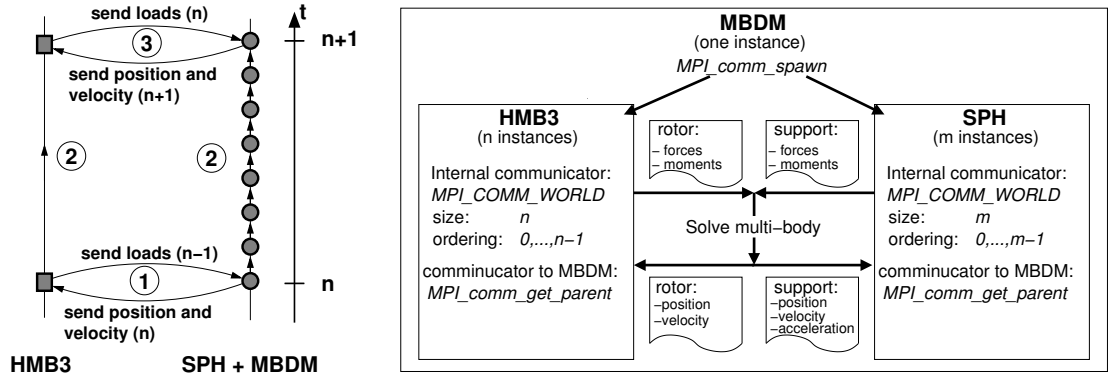

(a) the parallel conventional staggered method

(b) flow chart of the MPI implementation

Fig. 1. Employed couplign scheme: (a) the parallel conventional staggered method employed in present work; (b) flow chart of the MPI implementation and data exchange for coupled model [20].

At the beginning of each synchronisation time step, the position and velocities of the wind turbine rotor are transferred to the HMB3 aerodynamic solver, and forces and moments on the rotor are passed to the SPH. The two solvers are then advancing to a new time level with different methods and different number of steps. SPH performs 100 symplectic steps, while HMB3 performs 350 implicit pseudo-time steps. During the symplectic steps of the SPH code, the aerodynamic loads are kept constant (frozen). In return, the position and velocities of the rotor are kept constant during the implicit steps of HMB3. Once the synchronisation point is reached, the new position and velocities of all bodies, and rotor loads are obtained. Then, the algorithm proceeds to the new time level and information between the solvers is exchanged.

In the present work, the communication between the solvers was established through the Message Passing Interface (MPI), where the MBDM is executed as a single process and is dedicated to start SPH and HMB3 parallel solvers. The data flow diagram of the implementation is presented in Figure 1(b).

3. Test case description

A 10-MW wind turbine documented by [23] is used in this work. The rotor diameter is $178.3m$, and the wind turbine operates at a wind speed of $11m/s$ with a rotational speed of $8.824rpm$. The wind turbine is attached to the floating support which consists of three cylindrical floats that increase the buoyancy and stability of the structure. A schematic of the studied FOWT is shown in Figure 2(b).

In the present model, the FOWT is represented by three mooring lines and two bodies. The first body represents the rotor (three blades with the spinner), and the second body represents the combined nacelle, tower and floating support rigidly linked to each other. The two bodies are connected by a revolute joint and a constraint of constant rotational speed is applied to the rotor. The resulting system has 6 unconstrained degrees of freedom. The mechanical properties of the bodies and mooring lines are presented in Table 1.

The FOWT is placed in a shallow tank presented in Figure 2(b). The waves are generated using a paddle on one side, and dissipated using a beach-like slope on the other side of the tank. Waves are generated to represent the

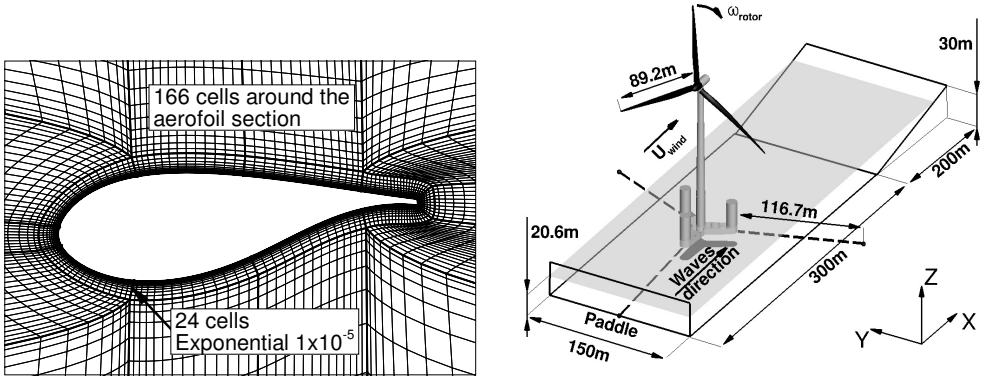

(a) Slice through 8*mln* mesh used to solve for aerodynamic loads. (b) Schematic of the employed model of FOWT.

Fig. 2. Coupled test case: (a) slice through 8*mln* mesh used to solve for aerodynamic loads; (b) schematic of the employed model of FOWT. Model consists of three mooring lines and two rigid bodies: the rotor (black) and combined body representing nacelle, tower and support (grey). Mooring lines are shown with dashed lines.

Table 1. Mechanical properties of the employed bodies and mooring lines.

Rotor	
Mass $[kg]$	$227,962$
Inertia tensor $[kg \cdot m^2]$	$\begin{bmatrix} 1.56 \cdot 10^8 & 0 & 0 \\ 0 & 7.84 \cdot 10^7 & 0 \\ 0 & 0 & 7.84 \cdot 10^7 \end{bmatrix}$
Nacelle, support and tower	
Mass $[kg]$	$4,223,938$
Inertia tensor $[kg \cdot m^2]$	$\begin{bmatrix} 2.03 \cdot 10^{10} & 0 & 0 \\ 0 & 2.03 \cdot 10^{10} & 0 \\ 0 & 0 & 2.81 \cdot 10^9 \end{bmatrix}$
Mooring lines	
Angle between adjacent lines $[°]$	120.0
Depth of anchors below SWL $[m]$	20.6
Depth of fairleads below SWL $[m]$	7.0
Length of the relaxed line $[m]$	116.73
Mooring line extensional stiffness $[N/m]$	$400 \cdot 10^6$
Mooring line damping coefficient $[Ns/m]$	$40,000$

specific sea state corresponding to a given wind speed. Based on the measurements of annual sea state occurrences in the North Atlantic and North Pacific [24], the wind speed of $11m/s$ corresponds to a sea state 4 with a mean wave height of $1.88m$ and a period of $8.8s$.

The aerodynamic grid consists of the rotor and nacelle *i.e.* the tower is not included and the effect of the blade passing on the tower is not investigated. The grid consists of 8*mln* cells, and the distribution of the grid nodes in vicinity to the blade surface is presented in Figure 2(a). The hydrodynamic domain is resolved using 5*mln* particles with initial uniform spacing of $0.625m$. Each of the solvers was executed separately before coupling to obtain a periodic solution of the loads. Once the initial conditions were obtained, the coupled computation was initiated.

4. Results

Results of the coupled computation are presented in Figure 3. The aerodynamic forces of the rotor as function of time are shown in Figure 4(a). As can be seen, the FOWT moves in the direction of the thrust by about $0.25m$ (displacement in x, surge), and sinks in water with a dynamic maximum of about $1m$ (displacement in z, heave).

The pitching motion is a result of combined action of thrust and waves, and maximum dynamic pitch is $0.12rad$ or 6.9 degrees (rotation about y axis, pitch). As wind turbine pitches under the the thrust force, the rotor moves in the direction of the wind (velocity in x direction in Figure 4(b)). In return, the aerodynamic force decreases due to the smaller inflow speed and the orientation of the rotor disk. As the applied force is reduced, the rotor velocity decreases. The inverse relation between the thrust force and x velocity of the hub is clear in Figure 4. The initial motion of the FOWT is dominated by the disbalance of the forces due to applied thrust, and the effect of the first wave passage is not visible. However, as a second wave approaches the support, additional positive moment about y axis is created, and is clearly visible in Figure 3(f). The conesecutive passages of the waves lead to a periodic pitching motion of the FOWT. Figure 5 presents different position of the FOWT during the computation. The wave breaking effect of the support structure is visible, and the recovery of the waves behind the FOWT can also be seen. The change of the pressure on the rotor can also be observed, especially at the tip of the nacelle.

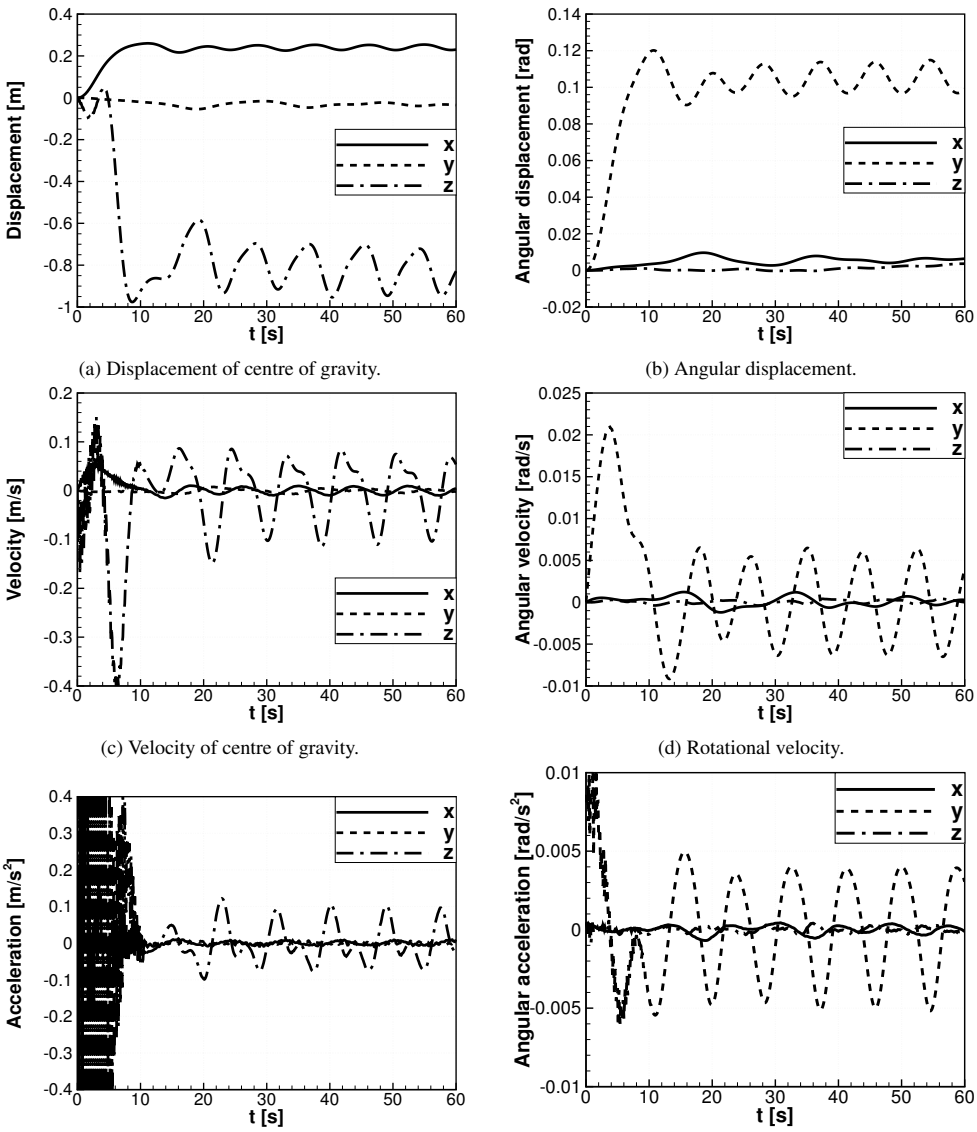

(a) Displacement of centre of gravity.

(b) Angular displacement.

(c) Velocity of centre of gravity.

(d) Rotational velocity.

(e) Acceleration of centre of gravity.

(f) Rotational acceleration.

Fig. 3. Lateral and rotational dynamics of the support platform for coupled test case.

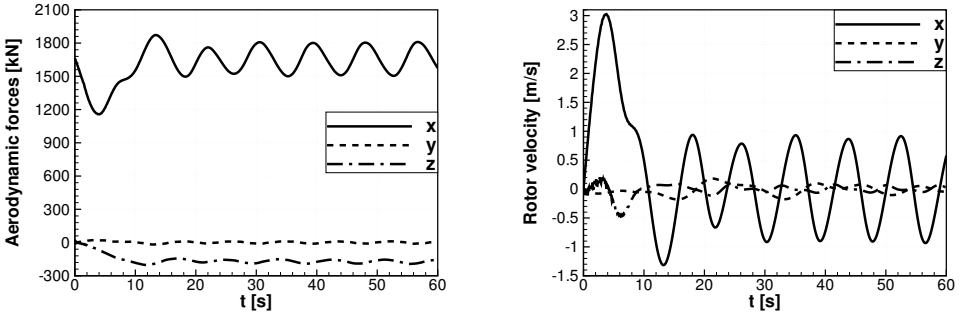

(a) Aerodynamic forces acting on the rotor.

(b) Velocity of centre of gravity of the rotor.

Fig. 4. Thrust of the rotor and velocity of centre of gravity of the rotor as function of time for coupled computation.

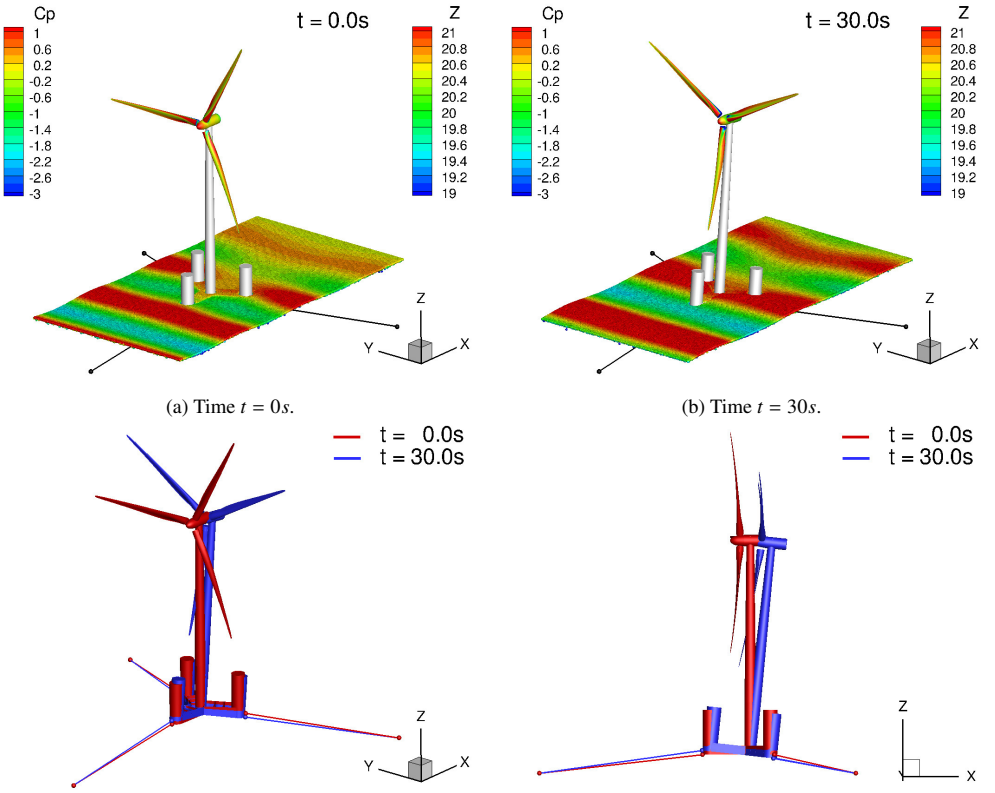

(a) Time $t = 0s$.

(b) Time $t = 30s$.

(c) Isometric view of position at times $t = 0s$ and $t = 30s$.

(d) Side view of position at times $t = 0s$ and $t = 30s$.

Fig. 5. Position and orientation of the FOWT at times $t = 0s$ and $t = 30s$ during coupled computation. Contours on the rotor correspond to pressure coefficient Cp, contours on the water surface correspond to surface elevation z in meters [20].

5. Conclusions

The paper presented a coupling method for the analysis of offshore wind turbines. The HMB3 CFD solver was used for the analysis of blade aerodynamics, and via a multi-body dynamics method it was coupled to a smoothed particle hydrodynamics tool to model the floating part of the turbine. The results showed that the weak coupling method put

forward in this paper is adequate for the solution of the problem at hand. The work could be further improved by comparison to the experimental data for a coupled system, since now validation was only possible for the components of the model.

Acknowledgements

The financial support of the Marie Curie Host Fellowships Program: FP7 - PEOPLE - 2012 - ITN - 309395 - New Materials And Reliability In Offshore Wind Turbines Technology "MARE-WINT" is gratefully acknowledged. Results were obtained using the EPSRC funded ARCHIE-WeSt High Performance Computer (www.archie-west.ac.uk). EPSRC grant no. EP/K000586/1.

References

[1] Corbetta, G., Mbistrova, A.. The European offshore wind industry - key trends and statistics 2014. Report; European Wind Energy Association, EWEA; 2015.

[2] Ho, A., Mbistrova, A.. The European offshore wind industry - key trends and statistics 1st half 2015. Report; European Wind Energy Association, EWEA; 2015.

[3] Corbetta, G., Ho, A., Pineda, I., Ruby, K., Van de Velde, L., Bickley, J.. Wind energy scenarios for 2030. Report; European Wind Energy Association, EWEA; 2015.

[4] Fried, L., Qiao, L., Sawyer, S., Shukla, S., Bitter, L.. Global wind report 2014: Annual market update. Online; Global Wind Energy Council, GWEC; 2014. URL: http://www.gwec.net/publications/global-wind-report-2/global-wind-report-2014-annual-market-update; Retrieved: 03/30/2016.

[5] Arapogianni, A., Genachte, A.B., Ochagavia, R.M., Vergara, J.P., Castell, D., Tsouroukdissian, A.R., et al. Deep water - The next step for offshore wind energy. Report; European Wind Energy Association, EWEA; 2013.

[6] Barakos, G., Steijl, R., Badcock, K., Brocklehurst, A.. Development of cfd capability for full helicopter engineering analysis. In: 31st European Rotorcraft Forum. 2005,Paper No. 91.

[7] Gomez-Gesteira, M., Rogers, B.D., Crespo, A.J.C., Dalrymple, R.A., Narayanaswamy, M., Dominguez, J.M.. Sphysics - development of a free-surface fluid solver - part 1: Theory and formulations. Computers & Geosciences 2012;48:289–299. URL: http://dx.doi.org/10.1016/j.cageo.2012.02.029. doi:10.1016/j.cageo.2012.02.029.

[8] Woodgate, M.A., Barakos, G.N., Scrase, N., Neville, T.. Simulation of helicopter ditching using smoothed particle hydrodynamics. In: 39th European Rotorcraft Forum. 2013,.

[9] Dehaeze, F., Barakos, G.N.. Hovering rotor computations using an aeroelastic blade model. The Aeronautical Journal 2012;116(1180):621–650.

[10] Dehaeze, F., Barakos, G.N.. Mesh Deformation Method for Rotor Flows. Journal of Aircraft 2012;49(1):82–92. URL: http://arc.aiaa.org/doi/abs/10.2514/1.C031251. doi:10.2514/1.C031251.

[11] Carrión, M., Steijl, R., Woodgate, M., Barakos, G., Munduate, X., Gomez-Iradi, S.. Aeroelastic analysis of wind turbines using a tightly coupled CFD-CSD method. Journal of Fluids and Structures 2014;50:392 – 415. URL: http://dx.doi.org/10.1016/j.jfluidstructs.2014.06.029. doi:/10.1016/j.jfluidstructs.2014.06.029.

[12] Jameson, A.. Time dependent calculations using multigrid, with applications to unsteady flows past airfoils and wings. In: 10th Computational Fluid Dynamics Conference. American Institute of Aeronautics and Astronautics; 1991,doi:10.2514/6.1991-1596.

[13] Spalart, P.R., Jou, W., Strelets, M., Allmaras, S.R.. Comments on the Feasibility of LES for Wings, and on a Hybrid RANS/LES Approach. In: Proceedings of the First AFOSR International Conference on DNS/LES. 1997,.

[14] Savenije, L.B., Ashuri, T., Bussel, G.J.W., Staerdahl, J.W.. Dynamic modeling of a spar-type floating offshore wind turbine. In: Scientific Proceedings European Wind Energy Conference & Exhibition. 2010,.

[15] Nikravesh, P.E.. Computer-aided Analysis of Mechanical Systems. Upper Saddle River, NJ, USA: Prentice-Hall, Inc.; 1988. ISBN 0-13-164220-0.

[16] Haug, E.J.. Computer Aided Kinematics and Dynamics of Mechanical Systems. Vol. 1: Basic Methods. Needham Heights, MA, USA: Allyn & Bacon, Inc.; 1989. ISBN 0-205-11669-8.

[17] Gómez-Iradi, S., Steijl, R., Barakos, G.N.. Development and validation of a cfd technique for the aerodynamic analysis of hawt. Journal of Solar Energy Engineering 2009;131(3):031009. doi:10.1115/1.3139144.

[18] Carrión, M., Steijl, R., Woodgate, M., Barakos, G., Munduate, X., Gomez-Iradi, S.. Computational fluid dynamics analysis of the wake behind the mexico rotor in axial flow conditions. Wind Energy 2014;URL: http://dx.doi.org/10.1002/we.1745. doi:10.1002/we.1745.

[19] Greenhow, M., Lin, W.M.. Nonlinear-free surface effects: Experiments and theory. Technical Report 83-19; MIT, Dept. of Ocean Engineering; 1983.

[20] Leble, V., Barakos, G.. Demonstration of a coupled floating offshore wind turbine analysis with high-fidelity methods. Journal of Fluids and Structures 2016;62:272 – 293. URL: http://dx.doi.org/10.1016/j.jfluidstructs.2016.02.001. doi:10.1016/j.jfluidstructs.2016.02.001.

[21] Leimkuhler, B.J., Reich, S., Skeel, R.D.. Integration methods for molecular dynamics. In: In Mathematical Approaches To Biomolecular Structure And Dynamics, IMA Volumes In Mathematics And Its Applications. Springer; 1996, p. 161–185.

[22] Matthies, H.G., Niekamp, R., Steindorf, J.. Algorithms for strong coupling procedures. Computer Methods in Applied Mechanics and Engineering 2006;195(1718):2028 – 2049. doi:10.1016/j.cma.2004.11.032.
[23] Bak, C., Zahle, F., Bitsche, R., Kim, T., Yde, A., Henriksen, L.C., et al. Description of the DTU 10 MW Reference Wind Turbine. Technical Report I-0092; DTU Wind Energy; 2013.
[24] Lee, W.T., Bales, S.L., Sowby, S.E.. Standardized Wind and Wave Environments for North Pacific Ocean Areas. David W. Taylor Naval Ship Research and Development Center; 1985.